Preliminary Design of a Tandem-Wing Tail-Sitter UAV Using Multi-Disciplinary Design Optimisation

H. Stone, K.C. Wong
Department of Aeronautical Engineering,
University of Sydney, NSW 2006, Australia.

The optimisation of a tail-sitter UAV (Unmanned Aerial Vehicle) that uses a stall-tumble manoeuvre to transition from vertical to horizontal flight and a pull-up manoeuvre to regain the vertical is investigated. The tandem wing vehicle is controlled in the hover and vertical flight phases by prop-wash over wing mounted control surfaces. It represents an innovative and potentially simple solution to the dual requirements of VTOL (Vertical Take-off and Landing) and high speed forward flight by obviating the need for complex mechanical systems such as rotor heads or tilt-rotor systems.

Introduction

Take-off and landing have historically presented difficulties for UAVs. If a runway is employed, much of the operational flexibility that is desired of a UAV is lost. Other solutions such as catapults or rocket assistance for take-off, and nets or parachutes for landing impose substantial costs and problems of their own. Although rotary wing UAVs are not subject to these landing and take-off problems they suffer performance limitations in terms of range, endurance and maximum forward speed. Other proposals aimed at combining some or all of the helicopter's low speed flight characteristics with those of a normal aircraft include the tilt-rotor, tilt-wing and tilt-body. These vehicles, however, represent mechanically complex solutions, with attendant weight and cost penalties.

A potentially simpler solution for the UAV application (where there are no passengers and crew who like to stay upright) is the tail-sitter. In keeping with the basic simplicity of the tail-sitter configuration, hover control can be effected via normal wing-mounted control surfaces. Further simplifications and weight reductions can be achieved if the aircraft is allowed to transition from horizontal to vertical flight via a "stall-tumble" manoeuvre and to trade altitude for kinetic energy before recovering to horizontal flight. This obviates the need for high power-to-weight ratios which are required for a smooth transition. Further more, this particular flight profile dispenses with any requirement for large edge-on flows into the propeller disc and hence allows the use of normal variable-pitch propellers in preference to more complicated, fully articulated helicopter-like rotors.

Vehicle Description

The basic configuration of the vehicle considered in this paper is presented in Figure 1 and Figure 2, with a typical flight profile shown in Figure 3. It is essentially a tandem wing configuration with twin tractor propellers mounted on the aft main wing. During hover, the vehicle is controlled in "pitch" and "roll"[†] via elevon control surfaces on the wing which are submerged in the prop-wash of the propellers. The function of the forward wing/canard is essentially to pull the vehicles AC (aerodynamic centre) forward, which in turn requires the CG (centre of gravity) to be significantly forward of the wing. This allows the control forces generated by the elevons submerged in the propeller slipstream to give adequate moments for hover control of the vehicle. Yaw control of the vehicle is effected via fins and rudders attached to the nacelles and which are also submerged in the propeller slipstream. Additionally the tips of the fins provide the attachment point for the landing gear and hence determine the "footprint" of the vehicle on the ground.

[†] The terms "pitch", "roll" and "yaw" are used here in the same sense as for a conventional aircraft in a vertical attitude.

Figure 1: Plan View of Vehicle.

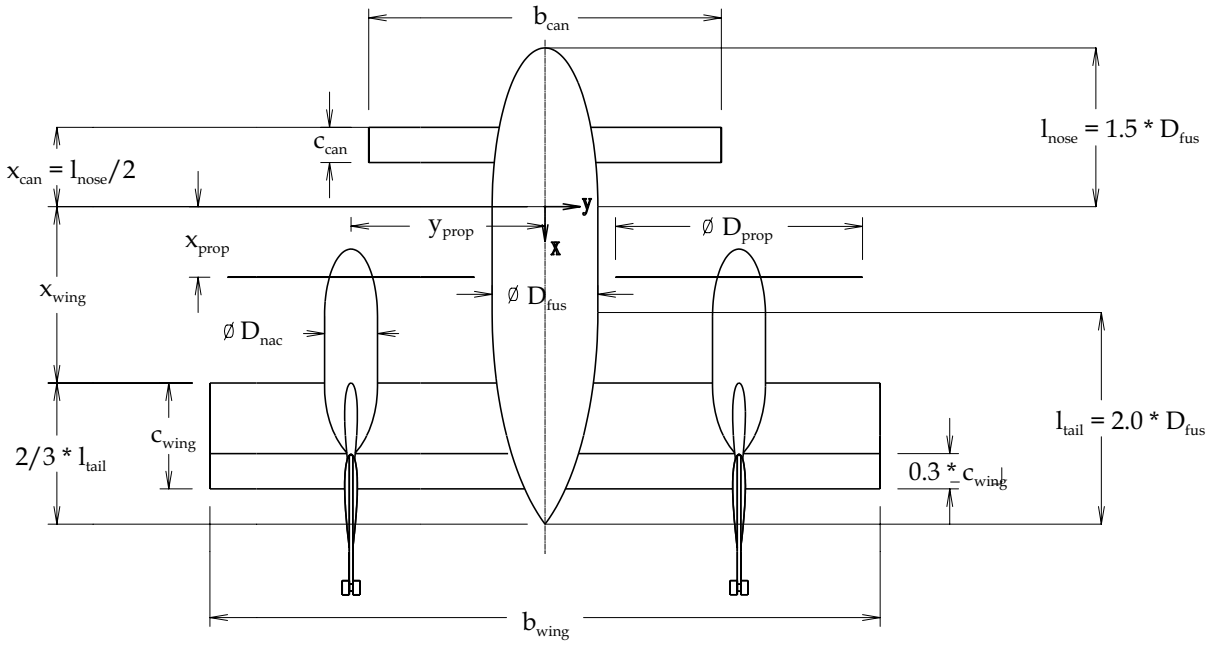

Figure 2: Side View of Vehicle.

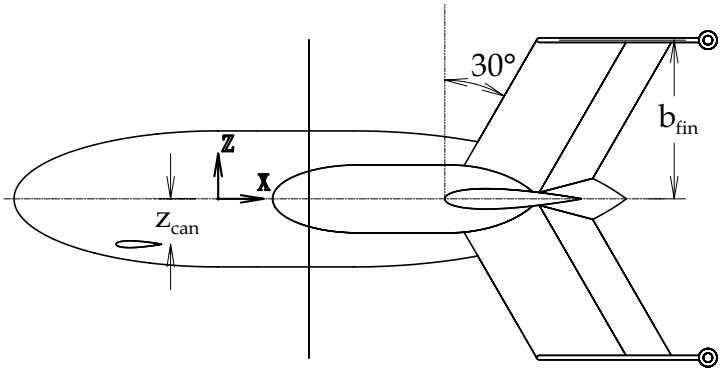

Figure 3: Typical Vehicle Flight Path.

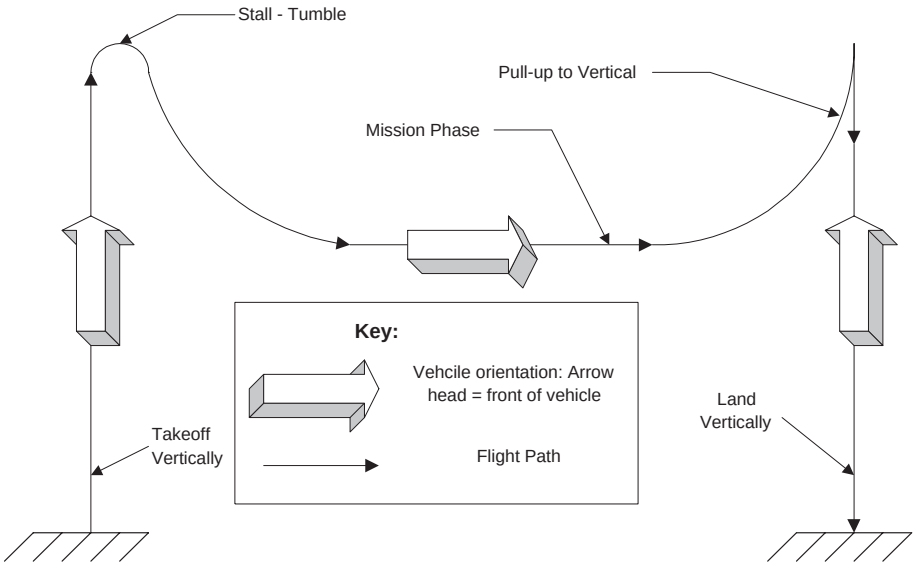

Major Design Issues

There are several unique design issues associated with this particular UAV.

- Hover Thrust Requirements: to take off and land vertically the total available thrust must exceed the vehicle weight by some reasonable margin (typically 15%[1]).
- Hover controllability: as this is achieved by using propwash over the wing mounted elevons, it is significantly affected by:
    1. the slipstream velocity distribution;
    2. the wing control surface geometry; and
    3. the position of the wing in relation to the vehicle CG.

  It should be further noted that the propeller slipstream velocity distribution is a function of the input power and blade shape parameters, such as diameter, chord and twist.
- Landing footprint: provision must be made for the vehicle to have an adequate ground footprint so that its minimum tip-over angle is less than some prescribed value (typically 20°).

These particular design considerations must also be balanced with more familiar requirements:

- static longitudinal and directional stability;
- structural integrity for flight and landing loads; and
- performance requirements in terms of range, endurance and maximum or minimum flight speeds.

Why optimisation?

Many of the above design requirements impose conflicting directives on the design. For instance, the propellers are required to operate efficiently at both high and low forward speeds; they are required to provide the flow over the elevons for low-speed controllability and they are required to provide thrust in excess of the vehicle's weight for take-off and landing. Altering propeller size and shape will affect all these parameters as well as engine power required and overall weight of the vehicle. In a similar manner, altering wing-shape and disposition relative to the canard and centre of gravity will affect low-speed controllability, high speed stability in addition to wing-loading and structural efficiency.

To resolve these conflicts a formal gradient-based optimisation procedure was employed, coupled with a parameterised model of the vehicle. The specific algorithm used was Sequential Quadratic Programming (SQP) as implemented in the MATLAB[2] Optimisation Toolbox. Minimisation of weight was used as the objective as this is reasonably expected to be related to total vehicle ownership costs. The solution was constrained by specifying minimum acceptable performance in terms of payload, range/endurance, maximum speed, structural integrity, hover controllability and various other factors. The vehicle was analysed using a combination of blade-element and panel methods for the propeller-wing aerodynamic interactions coupled with simple models for the structure, engine, controllability and weight.

It must be noted that all the significant design analysis inherent in the optimisation was based on physical models. The only use of statistical models were for simplistic factors outside the scope of configuration design such as engine weight to power ratios and the like.

Lastly it should be stated that this optimisation was conceived as a preliminary design tool, the purpose of which was to capture the driving forces in the design and the balance between them, rather than produce a final aeroplane.

Vehicle Model and Analysis

Design Variables and Key Parameters

The design of the vehicle was reduced to a mathematical model consisting of a series of design variables and fixed design parameters.

Design variables were used to describe:

- vehicle geometry (eg. wing span);
- propeller geometry (eg. blade diameter);
- control inputs (eg. canard incidence for cruise); and
- flight conditions (eg. cruise speed).

The design variables were available for alteration by the optimising program to obtain an optimum solution.

The fixed design parameters were used to represent relations that were assumed to be fixed throughout any given optimisation run. They included:

- geometric relations and constraints on the vehicle;
- certain performance requirements for the vehicle (eg. range and maximum speed);
- structural parameters relating to the vehicles assumed construction materials; and
- engine model relationships and assumptions (eg. the weight per horsepower that could be expected of typical UAV engines).

In essence, the fixed parameters either represented performance requirements that were later used to constrain the vehicle's design or critical assumptions about different parts of the vehicle model. By varying these parameters *between* optimisation runs, the

sensitivity of the vehicle design to a particular requirement or assumption could be analysed.
The design variables, $\underline{\mathbf{X}}$, and the key fixed parameter variables are listed in Table 1 and Table 2. The important geometric design variables and parameters are also shown in Figure 1 and Figure 2.

Table 1: Design Variables

$\mathbf{X}$ = *vector of design variables*

$$\mathbf{X} = \begin{bmatrix} \mathbf{X_t} \\ \mathbf{X_b} \\ \mathbf{X_f} \\ \mathbf{X_g} \\ \mathbf{X_s} \end{bmatrix} = \begin{Bmatrix} \text{Struct. thickness variables} \\ \text{Blade / propeller variables} \\ \text{Flight / other variables} \\ \text{Vehicle geometry variables} \\ \text{Slack Variables} \end{Bmatrix}$$

$$\mathbf{X_t} = \begin{bmatrix} t_{wing} \\ t_{can} \\ t_{fus} \\ t_{nac} \end{bmatrix} = \begin{Bmatrix} \text{Wing skin thickness} \\ \text{Canard skin thickness} \\ \text{Body skin thickness} \\ \text{Nacelle skin thickness} \end{Bmatrix}$$

$$\mathbf{X_f} = \begin{bmatrix} x_{pl} \\ \alpha_{cr} \\ \alpha_{V_{max}} \\ V_{cr} \end{bmatrix} = \begin{Bmatrix} \text{Payload fuselage station} \\ \text{Angle of Attack, Cruise} \\ \text{Angle of Attack, } V_{max} \\ \text{Cruise Speed} \end{Bmatrix}$$

$$\mathbf{X_g} = \begin{bmatrix} D_{fus} \\ b_{fin} \\ \delta_{can,cr} \\ \delta_{can,V_{max}} \\ x_{wing} \\ c_{wing} \\ c_{can} \\ b_{wing} \\ b_{can} \end{bmatrix} = \begin{Bmatrix} \text{Fusealge Diameter} \\ \text{Fin Span} \\ \text{Canard Angle, Cruise} \\ \text{Canard Angle, Max Speed} \\ \text{Wing leading edge station} \\ \text{Wing chord} \\ \text{Canard chord} \\ \text{Wing Span} \\ \text{Canard Span} \end{Bmatrix}$$

$$\mathbf{X_b} = \begin{bmatrix} x_b \\ y_b \\ D \\ p/D \\ w \\ \theta_h \\ \theta_{cr} \\ \theta_{V_{max}} \\ P_{max} \\ P_{cr} \\ D_{nac} \end{bmatrix} = \begin{Bmatrix} \text{Propeller x position} \\ \text{Propeller y position} \\ \text{Propeller diameter} \\ \text{Pitch: diameter ratio} \\ \text{Washout, root - to tip} \\ \text{Collective pitch - hover} \\ \text{Collective pitch - cruise} \\ \text{Collective pitch - } V_{max} \\ \text{Power at Hover and } V_{max} \\ \text{Power in cruise} \\ \text{Nacelle diameter} \end{Bmatrix}$$

$$\mathbf{X_s} = \begin{bmatrix} W_{to} \\ x_{cs} \end{bmatrix} = \begin{Bmatrix} \text{Tentative Takeoff Weight} \\ \text{Tentative Control System cg} \end{Bmatrix}$$

Table 2: Important Design Parameters

R = *range, (statute miles)*
E = *endurance, (hrs)*
V_{max} = *max speed requirement, (ft / sec)*
K_{hov} = *Hover thrust exceedance factor*
K_{eng} = *Engine Wt: Power ratio, (lbs / HP)*
K_{str} = *Structural Weight:Skin Weight ratio*
C_f = *Skin friction drag coefficient*
$c_{p,max}$ = *Specific HP fuel consumption at Max RPM, (lbs / hr / HP)*
w_{pl} = *Payload weight, (lbs)*
l_{pl} = *Payload length, (ft)*
h_{pl} = *Payload height and width, (ft)*
$\overline{x_{sm}}$ = *Minimum static margin (ref to wing chord)*

The above parameters represent only the MAJOR ones used. Many others describing structural and geometric characteristics of the vehicle and its operating environment were also included.

Propeller Model

The propeller was modelled using Goldstein's vortex blade element theory[3], coupled with measured 2-D airfoil data. The NACA 0012 airfoil was used for the blade section data as it was felt to be a "typical" airfoil and results were available for it at low Reynolds numbers ($5x10^5$) and over a complete range of angles of attack [-180°, +180°][4]. Mach number effects were accounted for in determining the 2-D section lift and drag coefficients.
The propeller model was used to predict thrust and power characteristics along with the induced velocities (both axial and tangential) added to the flow field by the action of the propeller. These velocities were only added in the hover flow-field case as they were felt to be of secondary importance at higher speeds.

The blade twist distribution was represented by the following equation:

$$\beta(x) = \tan^{-1}\left(\frac{p/D}{\pi \cdot x}\right) - w \cdot x + \theta$$

where:
x = *blade radial station* = r/R
r = *radial position on blade*
R = *blade radius*
p/D = *blade pitch: diameter ratio*
w = *linear blade washout*
θ = *blade collective pitch angle*
β = *local blade angle.*

The 2-D C_l vs alpha data was slightly modified by deleting the post-stall "C_l-trough" and maintaining a constant C_l above stall. This alteration gave better agreement with experimental results in the post-stall region

Aerodynamic Panel Model

A vortex-lattice fixed wake panel model was used to predict the aerodynamic characteristics of the vehicle. No account was made in the model for the fuselage and nacelles. (These were included, however, in the drag model of the vehicle). A picture of a typical aerodynamic grid is given in Figure 4.
The wing, canard and fins were assumed to be NACA 0015 sections. Section lift and drag characteristics, with and without elevon deflections, were predicted by standard techniques[5] and this data was used to correct the basic inviscid panel solution.

Figure 4: Typical Aerodynamic Panel Grid.

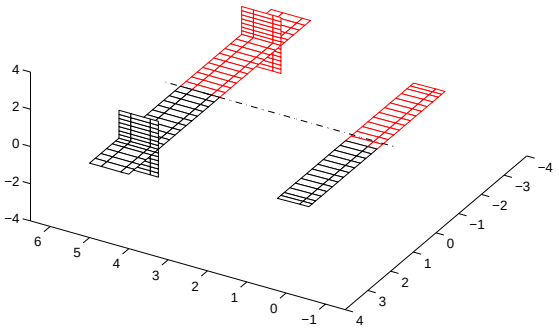

Aerodynamic Grid Considerations

In the standard vortex lattice model, the lifting surfaces are represented by finite numbers of bound and trailing vortices and the boundary condition of zero flow through the surface is applied at a finite number of control points. One problem with using vortex lattice methods in a gradient based optimisation is that if a *trailing* vortex of one surface lies near a control point of another then the solution becomes sensitive to movements of either the vortex or control point. This can cause invalid gradient information to be generated during the finite difference calculations as the span of the surfaces are moved small amounts relative to each other. This can even occur if the surfaces do not lie in the same plane. To overcome this problem the grids between all surfaces were aligned. For instance the wing and canard grids were aligned spanwise and the fin grid was aligned so that it had a panel edge at the same water-line (z-location) as the canard plane. Effectively this meant dividing the surfaces into a series of zones, the boundaries of which were determined by the projected edges of, or intersections with, other surfaces. These zones were then panelled in a consistent way to ensure alignment between grids on different surfaces.
Because the spanwise zone panelling was based on dividing each zone's length by a nominal panel span, it was also necessary to ensure that re-panelling of the zones (adjustment of the number of panels in each) was not performed during gradient calculations.
Similar problems affecting gradient calculations also occur with swept or tapered surfaces due to the projection of the *bound* vortices from one half of the surface passing near control points on the symmetric half. For the vehicle considered in this paper the sweep of the fins presented such a problem. Because of this, the fins were artificially unswept for the aerodynamic solution as only longitudinal aerodynamic parameters were being calculated. These were not significantly affected by the 30° fin sweep.

Wing-Propeller Interaction

One of the most important features of the present analysis is the interaction of the propeller and wing. As the vehicle depends on prop-wash over the wing-mounted elevons for its hover controllability, the accurate prediction of this interaction is critical to the successful design of the vehicle. The most important aspects of this analysis are presented below.

- The nacelles were assumed to have axes coincident with the chord of the wing. This meant that the axial and tangential components of propeller induced velocity were parallel and normal to the wing chord respectively.
- The propeller slipstream was assumed to affect the main wing only and not the canard. This is justified because induced flow velocities at the canard, in-front of the propeller are much smaller than those at the wing behind the propeller[‡].
- The propeller induced velocities (both axial and tangential) were added to the freestream velocity components to give the basic flow-field for the wing elements of the panel model.
- The effect of the wing and canard on the propeller flow field was ignored.
- The development of the slipstream (calculated at the mid-chord of the wing), which is dependent on the distance from the propeller disc was accounted

[‡] Note that both the wing and canard were constrained for practical reasons to lie no closer to the propeller disc than 0.5 and 0.75 propeller radii respectively.

for[3], as were the effects of the nacelle radius in enlarging the slipstream diameter[6] . The induced tangential velocities were increased in the propeller wake as the slipstream contracted to ensure conservation of angular momentum[6].

Typical lift and drag distributions for both wing and canard are shown for a cruise case in Figure 5, and for a hover case in Figure 6 (wing only). The propeller effects on the wing aerodynamic loads are visible in the latter figure. In fact they are the sole cause of the loads for the hover case.

Figure 5: Typical Wing and Canard Lift and Induced Drag (x5) Distributions - Cruise Case.

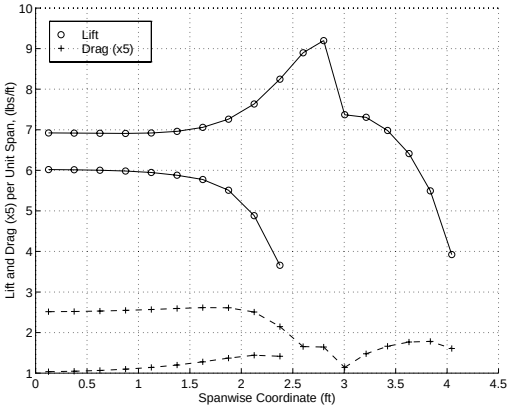

Figure 6: Typical Wing Only Lift and Induced Drag (x5) Distributions - Hover Case

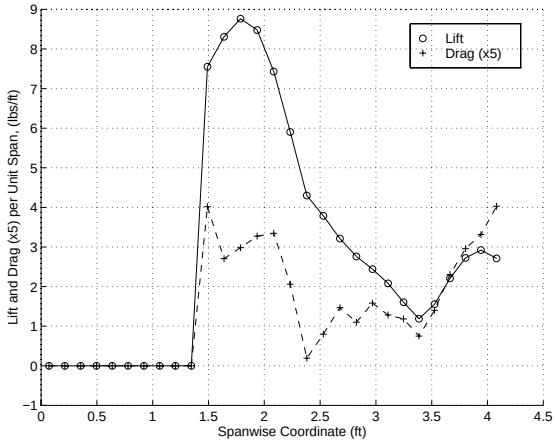

Treatment of Hover Velocity Discontinuity

When the propeller induced velocity profiles from the blade element program are added to the freestream velocities, a discontinuous flow-field is produced. The discontinuities in both velocity and angle of attack occur across the edges of the propeller slipstream, where the induced velocities typically go from their maximum values to zero. Although this situation is untenable physically (due to viscosity causing some mixing in the boundary region of the slipstream), the flow-field exhibits steep velocity and angle of attack profiles across this boundary.

When this discontinuous flow field is coupled with a vortex-lattice aerodynamic model there is an immediate and spurious sensitivity in the solution to the local grid geometry in the region of the discontinuity. This arises because the panel "sees" different input velocity values depending on which side of the discontinuity a particular panel control point lies. In the present case where the discontinuity occurs at the edge of a propeller slipstream, this means that a control point just within the slipstream will "see" a different velocity than one just outside it. As the slipstream or grid geometry is changed, spurious peaks and troughs will occur in the calculated aerodynamic loads as panels pass through the discontinuity.

This poses similar problems to those discussed before in relation to the necessity of grid-alignment between surfaces. Smoothing the edges of the discontinuity can lessen the severity of the resultant ripples in output quantities, such as lift and drag, but cannot totally eliminate them. This is because the panel control points are effectively sampling the velocity distribution at a fixed spatial frequency much lower than that used in the finite difference calculations. To eliminate this problem a separate panel zone on the wing was added with edges tied to the edges of the propeller slipstream. This zone was then allowed to expand, contract and move with the slipstream in response to changes in the various propeller variables (such as power, twist, diameter and position). As before, repanelling of this and all other zones was not allowed during finite difference calculations. (In other words the zone boundaries could move but the number of panels in each zone was held constant during finite differencing).

Engine Model

The required engine power for the vehicle is a function of the maximum RPM requirements and the propeller blade shape variables. It was assumed that whatever the final RPM/Power requirement, this could be met by gearing an engine with a suitable power output. The engine power as a function of RPM at full throttle was modelled using a simple polynomial[7] that has been found to give good agreement with many manufacturer's data.

By combining this with a linear throttle to power relation, and using a simple volumetric model for fuel consumption[8], it was possible to obtain the specific fuel consumption of the engine at differing RPM values.

To ensure that engine weight and size were also correctly accounted for in the optimisation process, simple empirical relations were obtained for:

- engine and gearbox weight as a function of power (initially set at 1.5 lbs/HP);
- engine frontal area as a function of power; and
- engine volume as a function of power.

The final relations that were used were determined from data for reciprocating engines ranging from 1 HP to 250 HP. It must be stressed that engines exhibit *wide variations* around any simple relation and consequently such relations are useful for preliminary design purposes only!

Structural Model

The aircraft was assumed to be built from typical aerospace carbon-fibre composite material. The major assumptions pertaining to the structural model are given below.

- All layups were assumed to be quasi-isotropic and constant thickness. In real-world structures with multiple load cases it is unlikely that highly directional laminates will be suitable. As well, the use of quasi-isotropic laminates simplifies the structural analysis and decreases the number of optimisation parameters
- The ultimate strain in either tension or compression was assumed to be 4000 μs.
- Constant, single thickness layups were assumed for all structural elements.
- Both wing and canard were assumed to be constant chord, constant thickness sections constructed with full-depth cores. The fuselage was assumed to be of sandwich construction with a prescribed core thickness. Due to the use of sandwich construction buckling was ignored as a structural concern.
- The UAV was designed to withstand flight load factors of ±6 g's, based on the maximum speed air-load distributions.
- Inertial loads arising from the mass of the wing and other items (engines, nacelles, fins, blades, landing gear) were accounted for. These produced bending moment relief as well as torsion loads on the wing structure.
- Although a wing divergence constraint was provided, no direct flutter/aeroelastic constraint was used. The wing was, however, limited to a maximum twist of 4° at ultimate load and the elevon hinge-line was limited to a maximum deflection of 10% of its length.
- Wing and canard strains, due to torsion and bending loads only, were evaluated at the critical bending moment points on these surfaces. Strains were checked in the 0° (spanwise), +45° and -45° directions at these critical locations. Fuselage and nacelle strains were also checked.
- The wing structure was also analysed for moments and loads imposed by landing forces. These were assumed to occur for two landing conditions. The first was a symmetric drop from a 4.0 ft height onto all four legs, while the second was a drop from 1.0 ft height onto one leg with a tip angle of 25°. The forces induced by these drop loadings were calculated assuming a 9.0" stroke for the landing gear legs. For these cases, wing strains were checked at the wing root leading edge.

Although the structural model is, by necessity, simplistic, it is considered that it gives a reasonable indication of the structural drivers in the design.

Drag Model

The drag model for the aircraft combined drag results from the panel-method aerodynamic model together with estimates of the extra drag due to the body, nacelles and surface imperfections. The lift dependent drag for the lifting surface configuration was obtained directly from the panel model solution. Viscous drag corrections in the panel code were calculated based on the local angles of attack of each chordwise strip of panels and look-up tables for 2-D drag data. The extra drag corrections due to the body , nacelles and surface imperfections were calculated as an average of a wetted area analysis and a simple component drag breakdown. In calculating this "extra drag" those components associated with the wing, canard and fins were halved due to the viscous drag corrections already present in the panel solution.

For the wetted area analysis a skin friction coefficient of .008 was used. This was considered a reasonable value for a small UAV and is considerably higher than typical values for clean light aircraft. For instance a Rutan Varieze has a skin-friction drag coefficient of ≈ .005, while a typical sailplane has a value of .003[9].

For the component drag model, standard drag estimation techniques[10 11] were used. As the tail of the fuselage had a prescribed fineness ratio of 2.0, no base drag increment was applied.

Control Model

The control model for the vehicle was based on the simplified free-body diagram shown in Figure 7. The basic case considered for determining hover controllability consisted of applying a sudden pitch displacement to the vehicle. The figure of merit used to judge controllability was the maximum excursion of the vehicle in the direction of the pitch displacement,

assuming immediate and instantaneous maximum deflection of the control surfaces to oppose the initial motion. In reality, the maximum excursion would be greater due to finite actuator time constants and the need to control the first overshoot in the opposite direction as well as the maximum initial excursion. Never the less, the above figure of merit is considered useful as a basis for comparison and for setting minimum vehicle requirements.

Figure 7: Hover Control Free Body Diagram of Vehicle

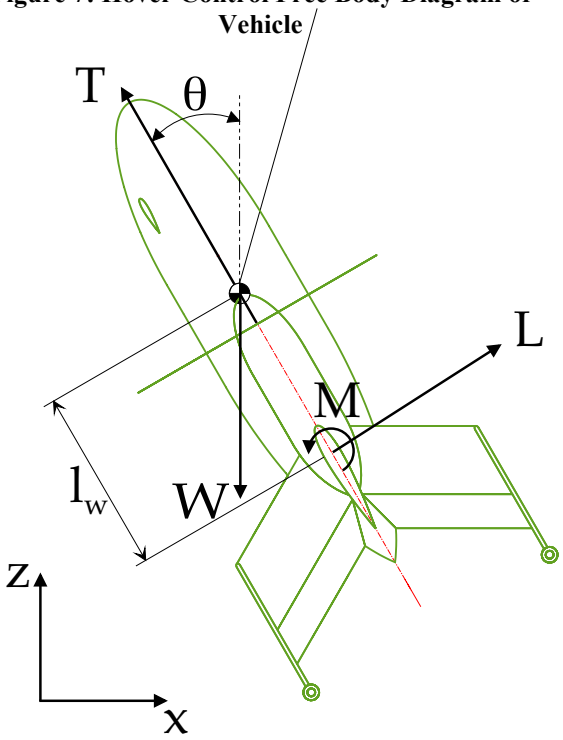

Important assumptions about the vehicle model were as follows.

- Conditions were assumed to be low-speed near hover.
- No body lift / drag forces were used.
- Flow in the propeller prop-wash region was assumed to remain axial.
- No lift or drag forces were generated by the canard or wing regions outside the propwash zones.
- The only significant forces accounted for were thrust, vehicle weight, wing normal force and pitching moment. The latter two forces arise from the deflected elevon control surfaces in the propeller slipstream.
- Body vertical motion was ignored and assumed easily controlled by slight thrust variations.

Using these assumptions it is possible to derive the force and moment balance differential equations and from these obtain a simple expression for the maximum excursion of the vehicle for a step tilt input. This expression is given below:

$$X_{me} = \frac{-1.5 \cdot \left[g\theta_0 + \left(L_{\delta max} / m \right) \right]^2}{g\left(L_{\delta max} l_w - M_{\delta max} \right) / I}$$

where:

g = *acceleration due to gravity*
X_{me} = *max negative excursion*
θ_0 = *initial " pitch" disturbance angle*
$L_{\delta max}$ = *wing normal force at* $\delta = \delta_{max}$
$M_{\delta max}$ = *pitching moment at* $\delta = \delta_{max}$, *(about CG)*
m = *vehicle mass*
I = *vehicle pitch inertia*
l_w = *distance between wing qtr chord and CG*
δ = *elevon deflection angle*

For typical cases the maximum pitch disturbance was set at 20°, with a maximum allowable excursion of 2.0 ft.

Weight Model

The empty weight, CG location and pitch inertia for the vehicle were calculated using a standard component weight breakdown. The structural weight was represented by the skin and core weights of the wing, canard, fins, fuselage and nacelles. These weights were determined from the component geometries and the structural thickness variables. This weight was then factored up by "K_{str}" (typ = 1.40) to account for the extra weight of fittings, attachments etc.,. Weights were also assigned for the landing gear (dependent on the take-off weight and length of legs); engines (linearly related to engine power) ; and a fixed weight of 15 lbs was allowed for the flight control system, sensors and miscellaneous items. The payload weight was an optimisation parameter and its position was an optimisation variable.

As typical UAV missions require the carriage of sophisticated electronic payloads the effects of vehicle and payload power requirements were included in the vehicle weight estimation. By specifying an average electrical power load for the mission (typ. 1000 W) adjustments to both the engine fuel consumption and to the engine size to support the total (aerodynamic and electrical) power requirements could be calculated.

Given the empty weight, it was possible to apply Breguet's range equation (modified somewhat due to electrical power usage) to find the fuel required to meet the range and endurance specifications. The most

critical of these set the fuel requirement for the aircraft. The fuel was assumed to be evenly distributed about the CG.

Organisation of Optimisation

At the heart of the optimisation process outlined in this paper is the *vehicle calculation function*, which calculates the objective (weight) and constraint values for a given set of design variables and parameters:

$$[f, \mathbf{g}] = vehicle(\mathbf{X}, \mathbf{P})$$

$\mathbf{X}$ = *vector of design variables*

$\mathbf{P}$ = *vector of design parameters*

f = *function value, (weight)*

$\mathbf{g}$ = *constraint vector*

= *vector formed from individual constraint equations*

$g_i < 0 \Rightarrow$ *constraint satisfied.*

Due to the need to calculate the function value and its finite difference gradients with respect to each design variable at each step, the basic *vehicle* function is called *at least* N+1 times per step (where N = number of variables). A flow diagram showing how a typical vehicle calculation proceeds is presented in Figure 8.

Various techniques were employed directly in the optimisation to minimise run times. For instance by saving all subroutine outputs for the vehicle calculation immediately preceding the finite difference evaluations and by tracking which variables affect which routines it is possible to skip the recalculation of parameters that will not be affected by the change of a particular variable.

It is also worth noting that all variables and constraints were normalised (by dividing by prescribed nominal values) to ensure a well-scaled design space.

Cost Function and Primary Constraints

The cost function used was the vehicle weight. A total of 50 constraints were used. The primary ones, (many of which have been mentioned before), are listed in Table 3.

Table 3: Vehicle Design Constraints

Constraint description	Number	Comments
Hover Thrust	1	Thrust must exceed vehicle weight by 15%.
Hover Controllability	1	Maximum excursion < 2.0 ft from equilibrium when disturbed by a 20° step tilt input.
Cruise and Max Speed Force Balance	6	Lift = Weight; Thrust = Drag; Vehicle must be in trim. (Both cases).
Static Stability	2	Longitudinal static margin > 5% for cruise and max speed cases.
Structural Loads (Flight Cases)	4	Wing, canard, body and nacelle maximum strains < 4000 μs.
Structural Loads (Landing)	2	Wing root strains for symmetric and unsymmetric drop cases < 4000 μs.
Wing Twist	1	Maximum wing twist < 4° at ultimate load.
Wing Hinge-line Deflection	1	Maximum hinge-line deflection < 10% of wing semi-span.
Skin Gauges	4	Wing, canard, nacelle and body facesheet gauges >= 0.015".
Volume Requirements	3	Payload, fuel and control system volumes must not intersect and must fit within vehicle.
Propeller clearances	3	Certain prescribed clearances from wing, canard and fuselage.
Engine size and volume	3	Engine must fit in nacelle in terms of total volume, frontal area and length.
Power consistency	1	Engine RPM in hover = engine RPM at max speed.
Ground Tip over angle	1	Fin size and CG location must ensure that tip over angle < 20°.
Weight consistency	1	Tentative MTOW = calculated MTOW. (Tentative MTOW is a slack variable to avoid iterations for MTOW.
Control system CG consistency	1	Tentative control system CG position = calculated position. (This is also a slack variable to avoid iteration).
Various other geometric and "sensible" constraints	15	Various clearance and positioning constraints (eg that the nacelles lie on the wings!) as well as reasonable constraints and bounds on variables.

.

Figure 8: Vehicle Calculation Flow Diagram

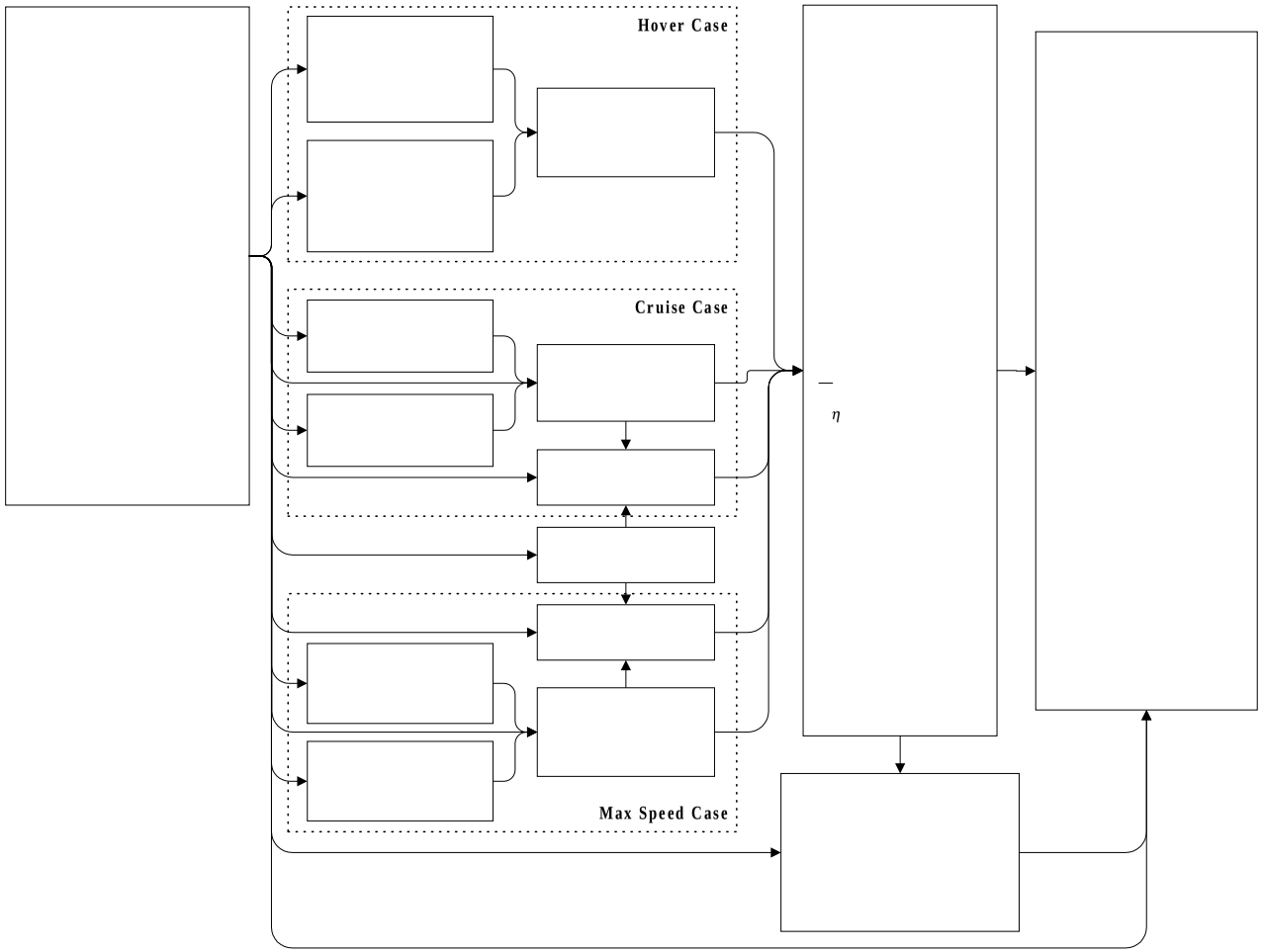

Results

The results so far demonstrate the usefulness of employing a formal optimisation technique for preliminary vehicle design. This is especially true for a vehicle which is of relatively novel configuration and which thus lacks the historical database associated with other designs. Without this data, configuration choices are less obvious, and the usefulness of an optimisation program based on "physical" calculations (as opposed to statistical relations) is enhanced.

While it is not possible to empirically test the results of the optimisation (short of building a vehicle), the designs produced by the current process satisfy "sanity check" calculations. Further more, benchmark testing of the individual program components, show that these give answers of an accuracy commensurate with their level of sophistication.

The convergence properties of the analysis were tested for a fixed set of parameters by starting from different semi-random positions in the design space. Final solution weights for these runs were within 1% of each other, and the maximum variations in the significant individual design variables were typically less than 5%. This was considered adequate for preliminary design purposes.

Plots of the convergence properties are shown in Figure 9 and Figure 10. These show the starting and end points of pairs of design variables[§] over a series of runs with the same parameters. The boxes in the figures enclose these start and end values and show the ability of the program to converge to similar solutions from markedly different initial positions. On the few occasions when the program failed to converge, this could usually be traced to exceptionally unrealistic combinations of certain initial variables.

Figure 9: Convergence of Take-off and Fuel Weights from Random Initial Guesses

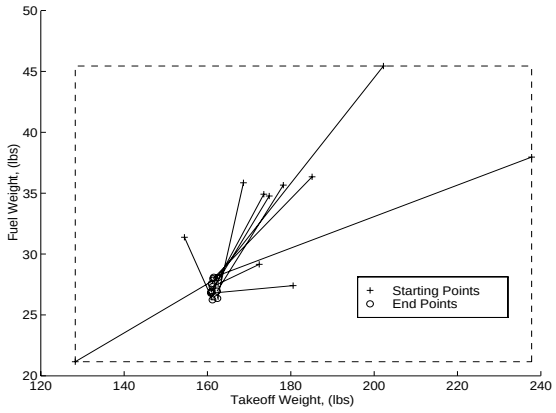

[§] Although technically the take-off and fuel weights are not optimisation variables, their values depend on them.

Figure 10: Convergence of Fuselage Length and Diameter from Random Starting Points

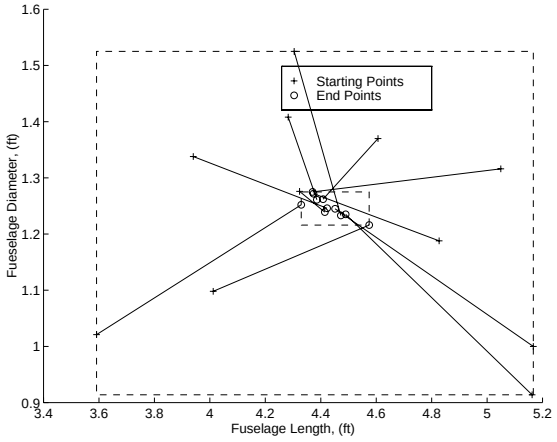

To speed up the optimisation many of the critical routines of the *vehicle* function were written in C (as MATLAB MEX files) rather than using normal MATLAB script files. This gave significant performance gains compared with direct MATLAB implementations. Typical run-times on a Pentium 133 MHz computer were in the range of 0.5 - 2.0 hrs compared to 10.0 hours before the implementation of the C coding[12].

The progress of a typical optimisation run is shown in Figure 11, while a typical vehicle plan view before and after optimisation is presented in Figure 12. The former of these figures tracks the relative changes in 6 of the most significant design variables from step to step in a typical optimisation run. Although in this case the optimiser took about 45 steps to reach practical convergence, in many other cases the number of steps was much less.

Figure 11: Variation in Normalised Variables Throughout a Typical Optimisation Run

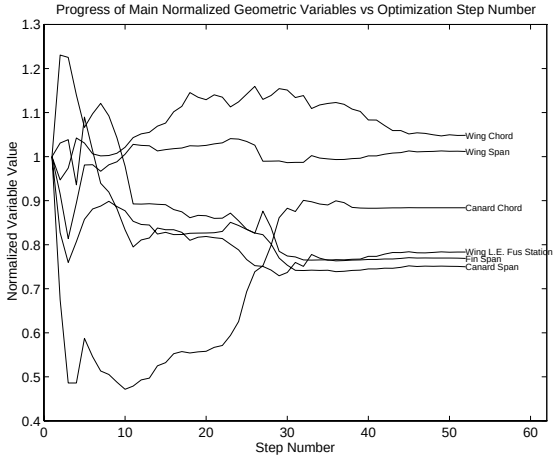

Figure 12: Typical Profiles Before and After Optimisation, (Dimensions in feet).

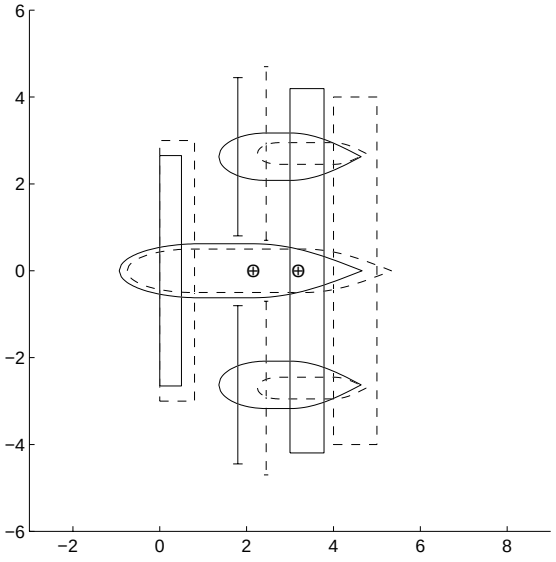

Vehicle Results

Several interesting observations about the configurations selected by the optimiser are appropriate:

- One of the predominant features of all the designs produced to date has been the clear preference for short fuselages. Although this results in sacrificing moment arm length for the wing control surfaces, this is more than offset by the reduction in pitch inertia in terms of meeting the hover control requirements.
- All the optimised configurations gravitated towards having alignment between the canard tip and the fin and propeller location. If the wing planform efficiency is plotted as a function of fin position for fixed wing and canard sizes this position corresponds to a local maximum.

The sensitivity of the vehicle design to range, payload, maximum speed, structural weight to skin weight ratio and engine weight to horsepower ratio were also investigated. Some of the results of these sensitivity studies are shown in the graphs below. For all the results, a baseline vehicle with the parameters shown in Table 4 was used.

Table 4: Baseline Parameter values

Parameter	Value
Range	400 miles
Payload	40 lbs
Maximum Speed	250 fps
Structural Weight: Skin Weight ratio	1.4
Engine Weight : Power Ratio	1.5 lbs/HP
Maximum Hover excursion (20° tilt input)	2.0 ft

Looking at the results it can be seen that the maximum speed requirement is a significant design driver. Changing this requirement from 225 ft/sec, (133 kts) to 300 ft/sec, (178 kts), more than doubles the vehicle weight. It would appear that this is largely due to the trade-offs associated with having to operate over a greater range of speeds. Because it is difficult to get a propeller to be efficient at both high speeds (requiring a small, highly twisted propeller) and also deliver sufficient thrust at low speeds (where a large, lowly twisted rotor is preferable), the optimiser is forced to add extra power which adds extra weight which then requires more power etc.,. It should be noted that the use of engines with lower power to weight ratios (eg turbo-shaft engines) would help to mitigate these problems.

Another feature of the optimised designs was the relatively high wing loadings that were obtained[**]. These were typically around 20 lbs/ft^2. The primary reason for this is that no low-speed flight requirements were imposed on the aircraft. Unlike other UAVs, this one is not required to take-off and land in a conventional manner and thus minimum forward speed ceases to be a design driver. The only constraint that was used was that the cruise angle of attack was limited to less than 3° below stall. It was noted that the vehicles often came close to this constraint boundary. The fact that this vehicle exhibits higher wing loadings than other UAVs is considered a positive benefit of the current design: it means that the vehicle is not forced to carry significant extra wetted area to satisfy landing and take-off constraints.

Other conclusions that can be made about the design's sensitivity to things such as engine weight to power ratio are largely self-explanatory.

Besides these individual points, the results clearly show that the proposed configuration is suitable for building small VTOL UAVs with maximum speeds up to 170 kts and ranges from 400 - 1500 statute miles or endurance's of between 6 and 18 hours. Such vehicles would have weights of between 130 and 400 lbs for a 40 lb payload.[††]

[**] Note that these loadings are relative to the combined wing and canard planform areas.

[††] For convenience simple polynomials or splines were used to provide trend-lines for the data in the following graphs. The real shape of any of the above relations may actually be more complex than the curves given. This would be especially true if different constraints were active in different regions of the graphs shown.

Figure 13: Take-off Weight vs Range

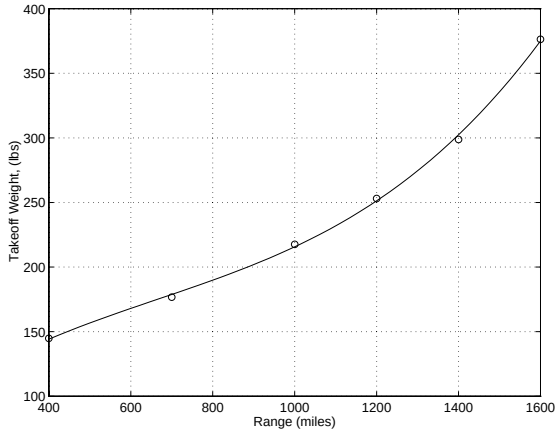

Figure 14: Take-off Weight vs Endurance

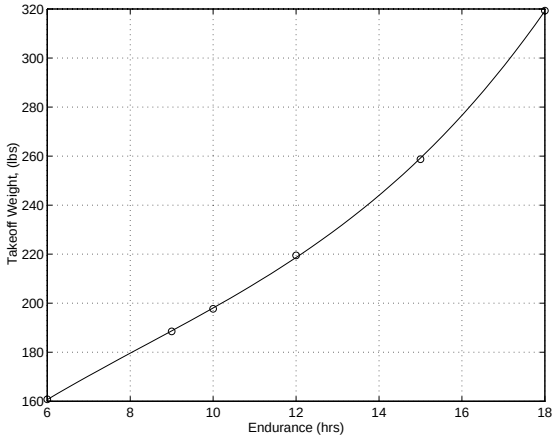

Figure 14: Take-off Weight vs Max Speed

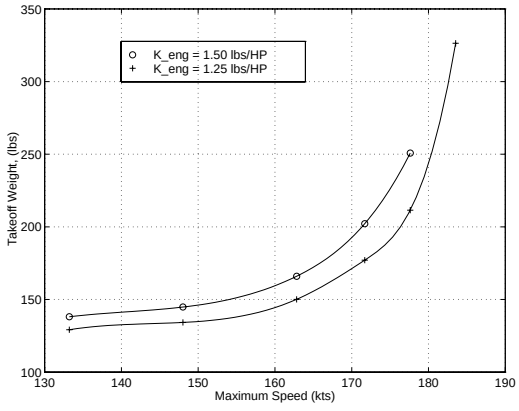

Figure 15: Wing and Canard Span plus Propeller Diameter vs Range

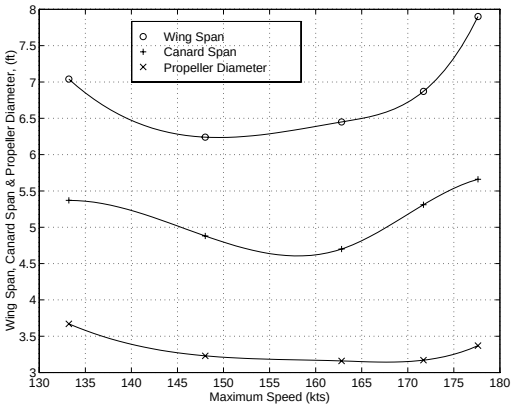

Further Work

Although much sensible data has been gained to date, there is scope for further improvement and refinement of the basic vehicle model on which the optimisation is based. Some specific areas of improvement are listed below.

- The aerodynamic model could be improved by inclusion of the fuselage and nacelles in the panel model. This would however involve a big increase in model size and run-times.
- The hover control figure of merit could be altered to reflect a more real world case, such as a wind gust disturbance rather than the presently used step tilt input.
- While wing flutter is not anticipated to be a problem with the current design (due to the engine mass being cantilevered well in front of the wing elastic axis), other important aeroelastic modes may exist. For instance, excessive wing twist or bending will cause the propeller thrust vector to move in relation to the aircraft CG, which may give rise to aeroelastic modes with coupling between wing flexure and body dynamics. This needs to be investigated further.

It may also be interesting to look at how size constraints affect the vehicle and whether it is possible to structure the vehicle design to allow for a "family" of aircraft with minimal changes between different models. All these should be possible with only minor alterations to the current analysis.

Conclusions

In conclusion it can be stated that the proposed configuration shows great promise in marrying the dual requirements of VTOL with efficient forward flight in a relatively simple design. The vehicle considered in this paper has shown itself to be a promising concept over a wide variety of missions and assumed parameter variations. The design also looks to be extensible to encompass other missions and larger payloads: this will be investigated in the future. Lastly, it is clear that the use of formal optimisation techniques in the preliminary design stage of this vehicle has been fruitful.

Figure 16: 3-D View of Typical Vehicle

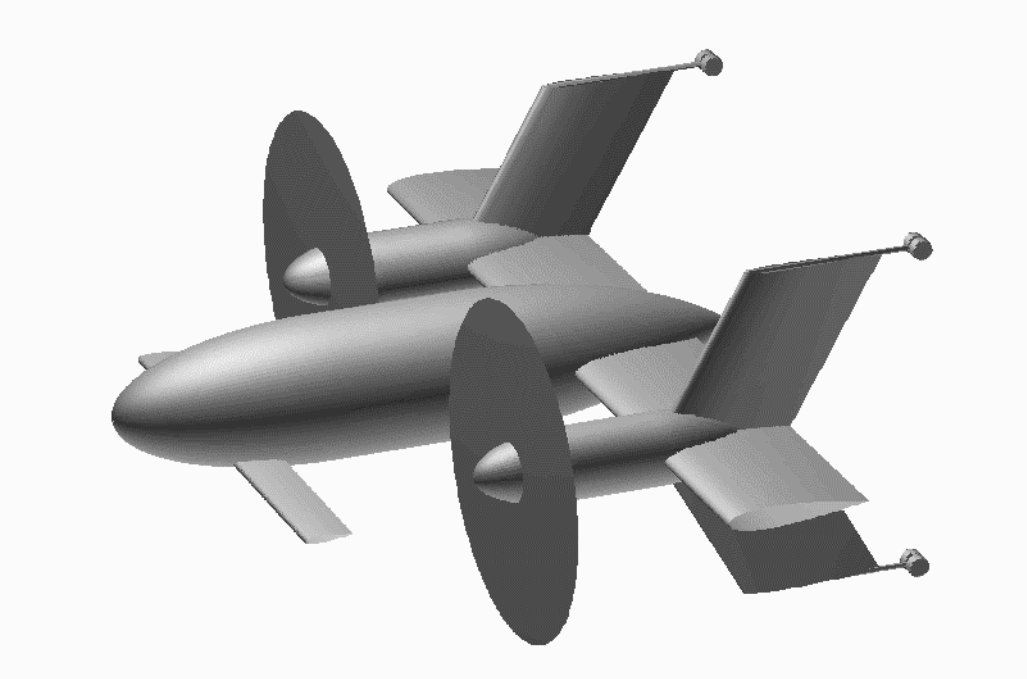

References

[1] Stoney, R.B., "Design, Fabrication and Test of a Vertical Attitude Take-off and Landing Unmanned Air Vehicle", Masters Thesis, Naval Postgraduate School, Monterey, Ca, 1993.

[2] MATLAB Optimization Toolbox, The Mathworks inc, 1992.

[3] McCormick, B.W., "Aerodynamics of V/STOL Flight", Academic Press, New York, 1969.

[4] Critzos, C.K., Heyson, H.H. and Boswinkle, R.W., "Aerodynamic Characteristics of NACA 0012 Airfoil Section At Angles of Attack From 0° to 180°", NACA TN3361, 1955.

[5] Roskam, J., "Airplane Design - Part VI: Preliminary Calculation of Aerodynamic, Thrust and Power Characteristics", Roskam Aviation 1990.

[6] McVeigh, M.A., Gray, L., Kisielowski, E., "Prediction of Span Loading of Straight-Wing/Propeller Combinations up to Stall", United Technology inc, NASA CR-2602, Oct 1975.

[7] Fiddes, S.P., and Hanrahan, M., "Optimum Propellers for RPVs", Eleventh International RPVs conference, University of Bristol, 1994, Paper No. 10.

[8] Durbin, E.J., and Dommasch, D.O., et al (eds) "NATO AGARD Flight Test Manual, Vol 1, Performance", Pergamon, 1962.

[9] Roskam, J., "Airplane Design - Part I: Preliminary Sizing of Airplanes", p118, Roskam Aviation 1990.

[10] McCormick, B.W., "Aerodynamics, Aeronautics and Flight Mechanics", John Wiley & Sons, 1979.

[11] Hoerner, S.F., "Fluid Dynamic Drag", Hoerner Fluid Dynamics, Albuquerque, N.M. 1965.

[12] Stone, H., Wong, K.C., "Preliminary Design of a Tandem-Wing Tail-Sitter UAV Using Multi-Disciplinary Design Optimisation", Proceedings of the Association of Unmanned Vehicle Systems International Conference 1996, p 163-178.